

Supporting Information

Microdroplet confined assembly enabling scalable synthesis of titania supported ultrasmall low-valent copper catalysts for efficient photocatalytic activation of peroxymonosulfate

Yi Zhang ^a, Ying Wang ^a, Xiangcheng Zhang ^a, Lei Wu ^a, Hao Wang ^a, Xiangru Wei ^a,
Winston Duo Wu ^a, Xiaoning Wang ^{a*}, Wei Li ^b, and Zhangxiong Wu ^{a*}

^a Particle Engineering Laboratory, School of Chemical and Environmental Engineering, College of Chemistry, Chemical Engineering and Materials Science, Soochow University, Suzhou City, Jiangsu 215123, P. R. China.

^b Department of Chemistry and Laboratory of Advanced Materials, Fudan University, Shanghai 200433, P. R. China

* Corresponding authors:

E-mail: wangxiaoning@suda.edu.cn (X. Wang), zhangwu@suda.edu.cn (Z. Wu)

1. Additional experiment details

Chemicals: Hydrochloric acid (HCl, ~ 37 wt%), sodium hydroxide (NaOH, in pellet form), absolute ethanol, $\text{Cu}(\text{NO}_3)_2 \cdot 3\text{H}_2\text{O}$ were obtained from Sinopharm Chemical Reagent Co., Ltd. (Shanghai, China). Titanium (IV) tetraisopropoxide (denoted as TTIP, 97 wt%), furfuryl alcohol (FFA, 98 %) and 2,2,6,6-tetramethyl-4-piperidinol (TEMP, 98 %) were obtained from Aladdin (Shanghai, China). Peroxymonosulfate (PMS, $\text{KHSO}_5 \cdot 0.5\text{KHSO}_4 \cdot 0.5\text{K}_2\text{SO}_4$) and the Pluronic triblock copolymer F127 (PEO–PPO–PEO, $M_w = 12500$) were obtained from Sigma-Aldrich. Methylene blue (MB) was purchased from J&K Chemical Ltd. (Shanghai, China). Iso-propyl alcohol (IPA) was obtained from Shanghai Lingfeng Chemical Reagent Co., Ltd. Tert-butanol (TBA, 99 %) was obtained from Shanghai Titan Scientific Co., Ltd. 5,5-Dimethyl-1-pyrroline N-Oxide (DMPO, 98 %) was obtained from Adamas Reagent Co., Ltd. All the chemical reagents were used as received without further purification. Deionized water was used whenever required.

Characterization and measurement: Powder wide-angle X-ray diffraction (XRD) patterns were acquired on a Bruker D2 PHASER diffractometer (Germany) by using the Cu $K\alpha$ (Ni filtered) radiation at a voltage of 30 kV and a current of 10 mA. Raman spectra were obtained on a laser Raman spectrometer (Renishaw UV-1000) with laser excitation energy of 532 nm. Scanning electron microscopy (SEM) images were taken by using a SU-1510 microscope (Hitachi High Technologies Corporation, Japan) or a ZEISS GeminiSEM 500. Transmission electron microscopy (TEM) images were

taken by using a FEI Tecnai F20 (America) TEM microscope equipping with the energy dispersive X-ray spectroscopy (EDX) element analysis. The high-resolution transmission electron microscopy (HRTEM) images were taken on a FEI Titan Cubed Themis G2 300 TEM equipped with a CEOS spherical (Cs) aberration corrector. The electron acceleration voltage was 300 kV. The particle size distributions of the various samples were acquired by analyzing SEM images containing over 150 individual particles by using Shineso (SHINESO, Hangzhou, China). Nitrogen adsorption/desorption isotherms were measured at -196 °C by using an ASAP 2020 sorption analyzer. The surface area was calculated by using the Brunauer-Emmett-Teller (BET) method. The pore volume was determined by the N₂ adsorbed amount at $P/P_0 = 0.99$, and the pore size distribution curve was obtained by using the Barrett-Joyner-Halenda (BJH) model. Before the measurement, the samples were degassed at 150 °C for at least 8.0 h under high vacuum. X-ray photoelectron spectroscopy (XPS) and auger electron spectroscopy (AES) were collected by using a VG Scientific ESCALAB 250Xi spectrometer (Thermo Fisher Scientific) with C 1s as the calibration standard line. The electron spin resonance (ESR) experiments were carried out on a JES-X320 spectrometer to characterize the oxygen vacancies and the valence states of the copper species in the samples, as well as to detect the reactive radicals generated over the photocatalytic degradation processes. In the detection of oxygen vacancies, a specific sample was loaded in a capillary tube. The ESR detection was conducted at a microwave frequency of 9.15 GHz, a microwave power 1.0 mW and a centerfield of 326 ± 50 mT at room temperature. For the detection of radicals, a 100

mM DMPO was adopted for capture of HO[•], SO₄^{•-} and O₂^{•-} radicals and a 100 mM TEMP was adopted for capture of ¹O₂. The ESR spectra were recorded at room temperature under the following operating conditions: a modulation frequency of 100 kHz, a sweep width of 0.5 mT, a microwave power of 1 mW, a microwave frequency of 9.15 GHz and a centerfield of 326.0 ± 5 mT, respectively. The optical properties of the samples were analyzed through the UV–vis diffuse reflectance spectra (DRS) by Shimadzu UV-3600.

Metal leaching, radical and intermediates identification: To evaluate the copper leaching of the catalyst after the photocatalytic reaction, the solution after filtration was analyzed with inductively coupled plasma optical emission spectrometry (5110 ICP-OES, Agilent Technologies) to determine the copper ion concentration.

To identify the active species involved in the heterogeneous photocatalytic PMS activation process, indirect quenching experiments were conducted by adding different radical scavengers with the Meso-CuO_x@TiO₂-8-350 sample as the representative catalyst. TBA was chosen as the HO[•] scavenger, IPA as the HO[•] and SO₄^{•-} scavenger, and FFA as the ¹O₂ scavenger. During a specific quenching experiment, 1.0 M TBA, 1.0 M IPA or 1.0 M FFA was added into the suspension before adsorption, followed by the same degradation procedure as described above. To determine the contribution of O₂^{•-} radicals for degradation, before light irradiation, the suspension was bubbled with pure N₂ for 30 min to remove the dissolved oxygen. After the addition of PMS and during the light irradiation, N₂ purging was proceeded

throughout the degradation process.

The intermediates generated during the degradation process of MB at different time intervals were identified by using an Agilent 1290 HPLC coupled with a 6545 Accurate-Mass QTOF system (LC-QTOF-MS). Chromatographic separation was performed on a ZORBAX Stable Bond C18 column (1.8 μm , 3.0 \times 50 mm). The column temperature was controlled at 30 $^{\circ}\text{C}$, and the injection volume was 5 μL . The mobile phase was a mixture of methanol (A) and 0.1% formic acid in water (B) at a flow rate of 0.3 mL min^{-1} . The gradient elution programs for the positive ions (i.e., $[\text{M}+\text{H}]^{+}$) were as follows. A: B (v: v) was 5%: 95% for the period of 0 ~ 0.5 min. Then, the A: B ratio was linearly increased to 100%: 0% in the period of 0.5 ~ 11 min and held for 2 min. After that, the A: B ratio was returned to 5%: 95% at the time point of 13.1 min and held for 4 min. The Dual AJS ESI ion source in the positive ion mode was set at the following conditions, namely, a drying gas temperature of 150 $^{\circ}\text{C}$, a drying gas flow rate of 10 L min^{-1} , a nebulizer pressure of 35 psi, a sheath gas temperature of 375 $^{\circ}\text{C}$, a sheath gas flow rate of 11 L min^{-1} , a capillary voltage of 3500 V, a nozzle voltage of 200 V and a fragmentor voltage of 125 V, respectively.

2. Additional Figures and tables

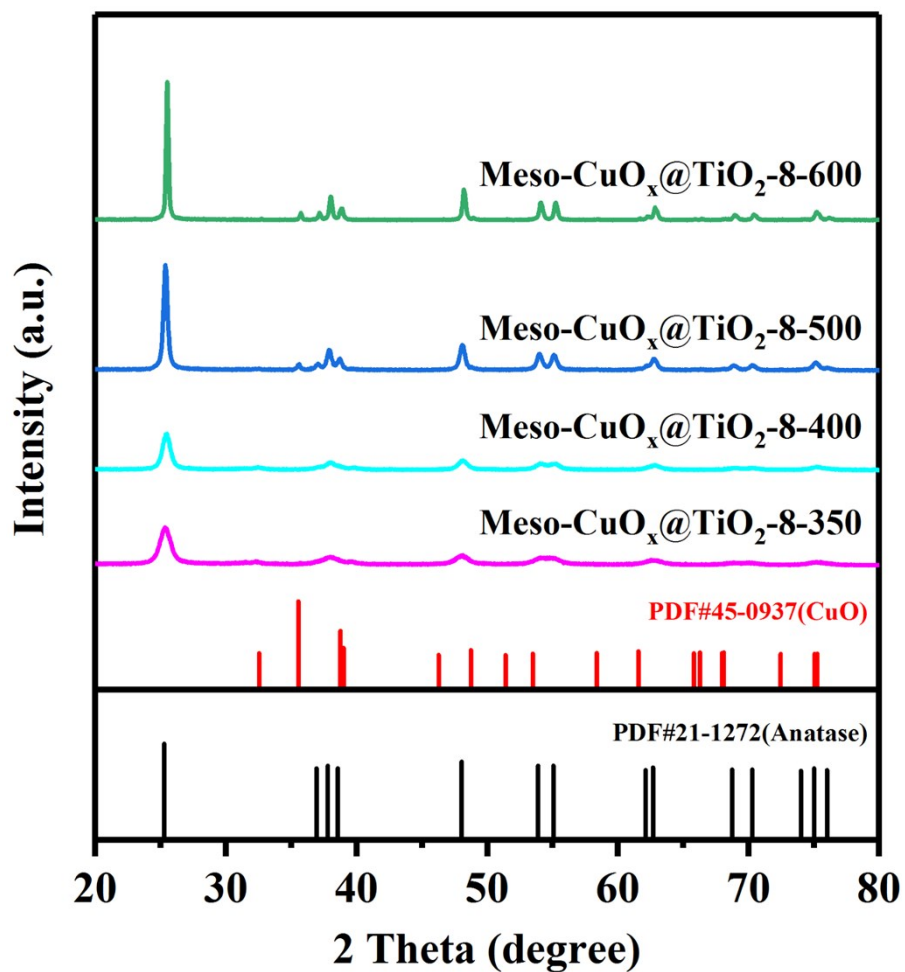


Fig. S1. XRD patterns of Meso-CuO_x@TiO₂-8-y obtained by calcination in air under different temperatures.

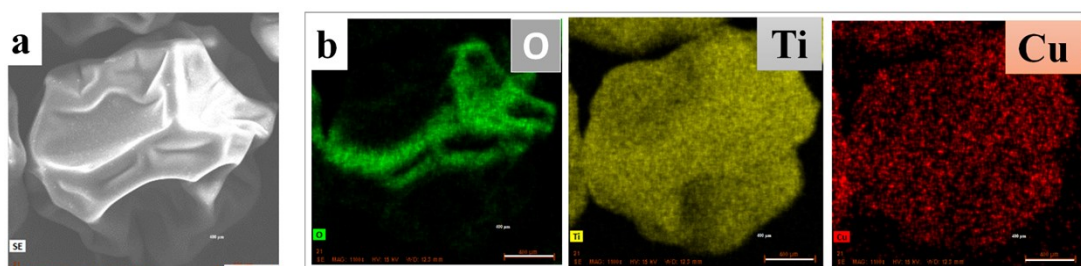


Fig. S2. Low-resolution SEM image and the corresponding elemental maps of Meso- $\text{CuO}_x@ \text{TiO}_2$ -8-350.

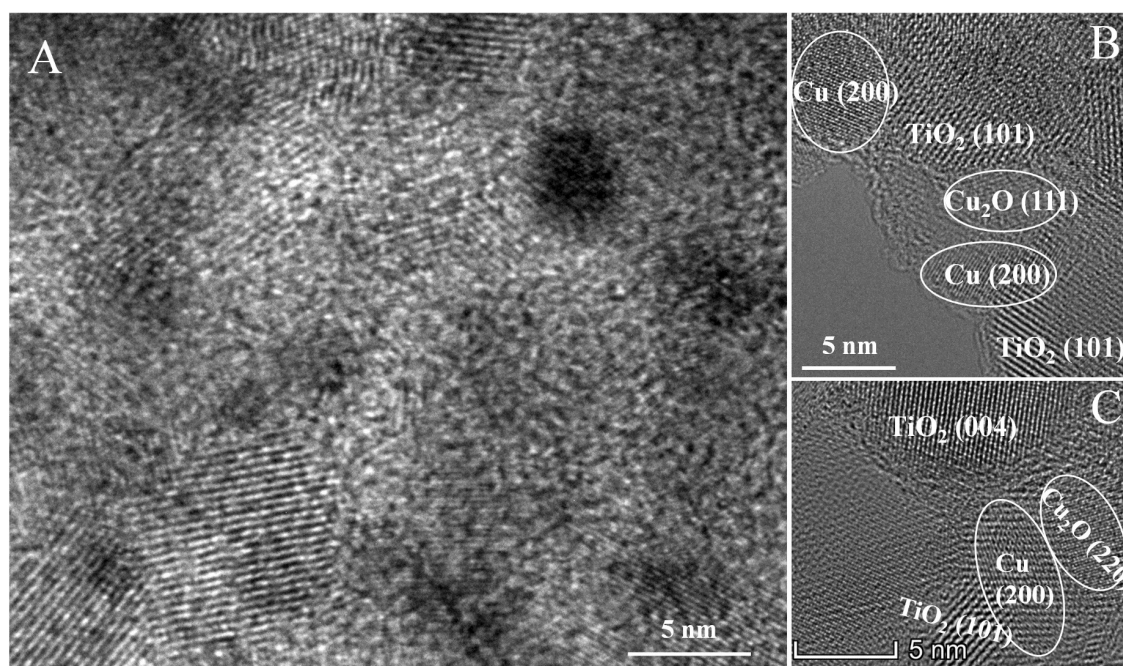


Fig. S3. Additional HRTEM and aberration-corrected HRTEM images of Meso-CuO_x@TiO₂-8-350 at various sample locations.

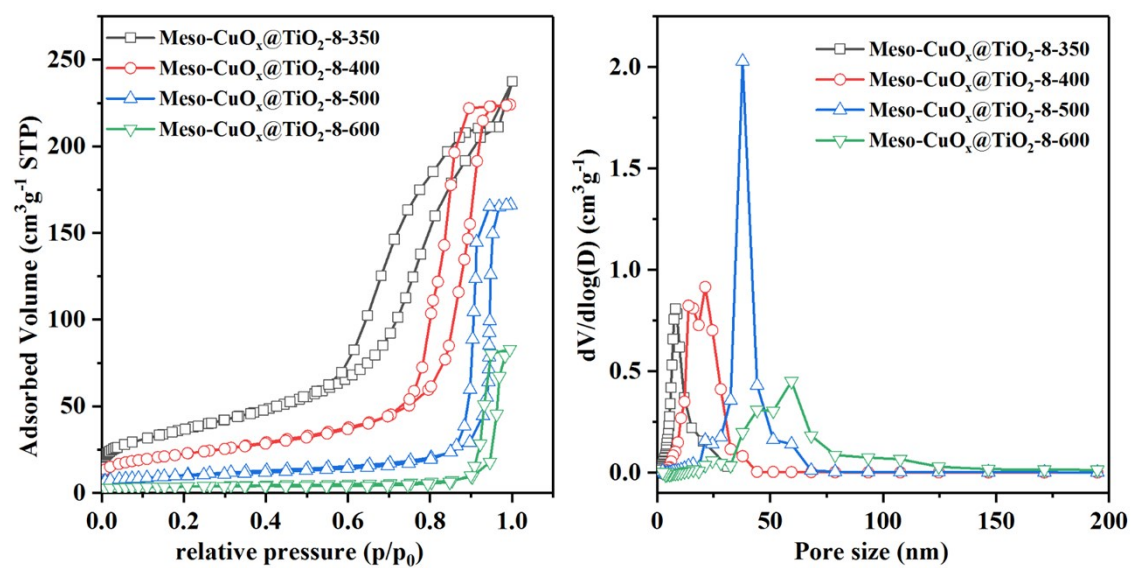


Fig. S4. N₂ sorption isotherms and the corresponding pore size distribution curves of Meso-CuO_x@TiO₂-8-y obtained by calcination in air under different temperatures.

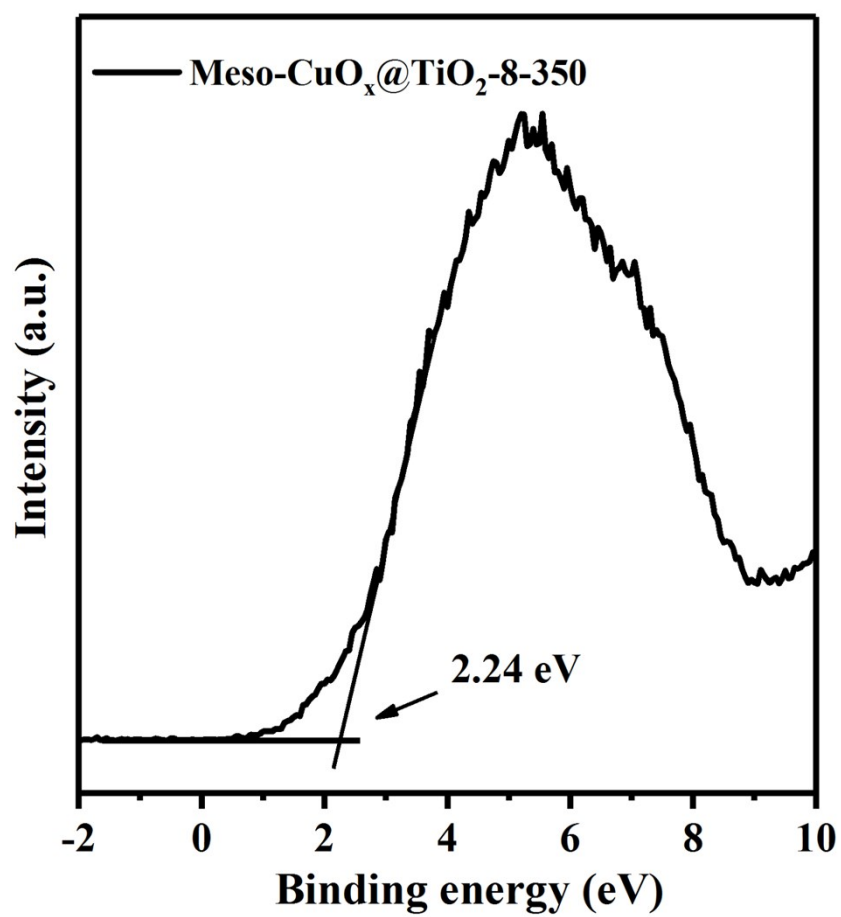


Fig. S5. Valence band XPS spectra of Meso-CuO_x@TiO₂-8-350.

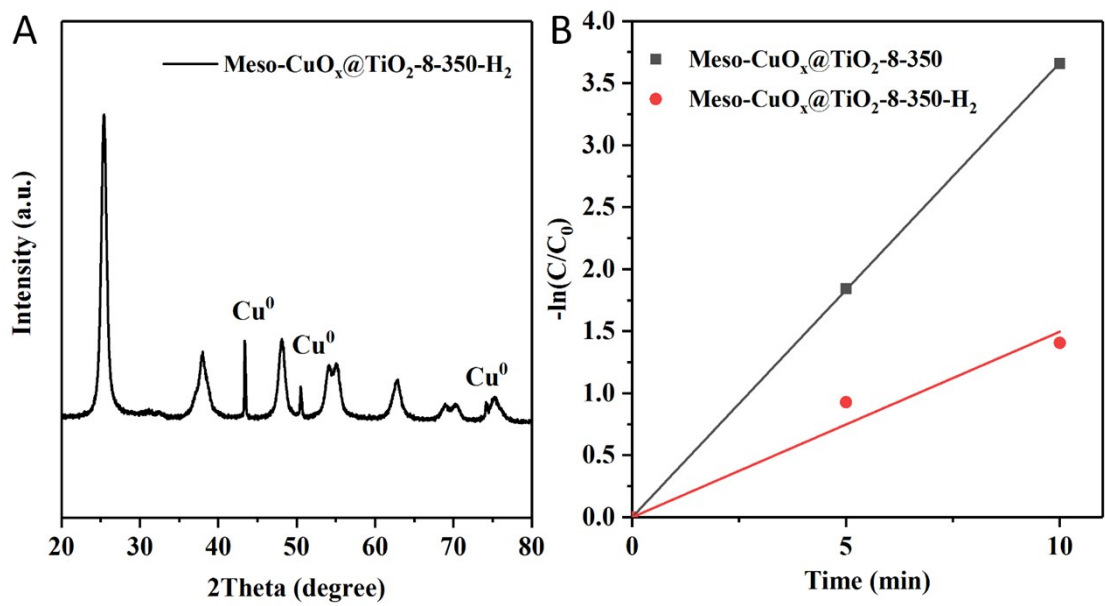


Fig. S6. XRD pattern (A) of Meso-CuO_x@TiO₂-8-350-H₂ obtained by calcination Meso-CuO_x@TiO₂-8-350 in H₂/Ar, and the MB degradation comparison (B) between Meso-CuO_x@TiO₂-8-350-H₂ and Meso-CuO_x@TiO₂-8-350 under the catalyst/PMS/light system.

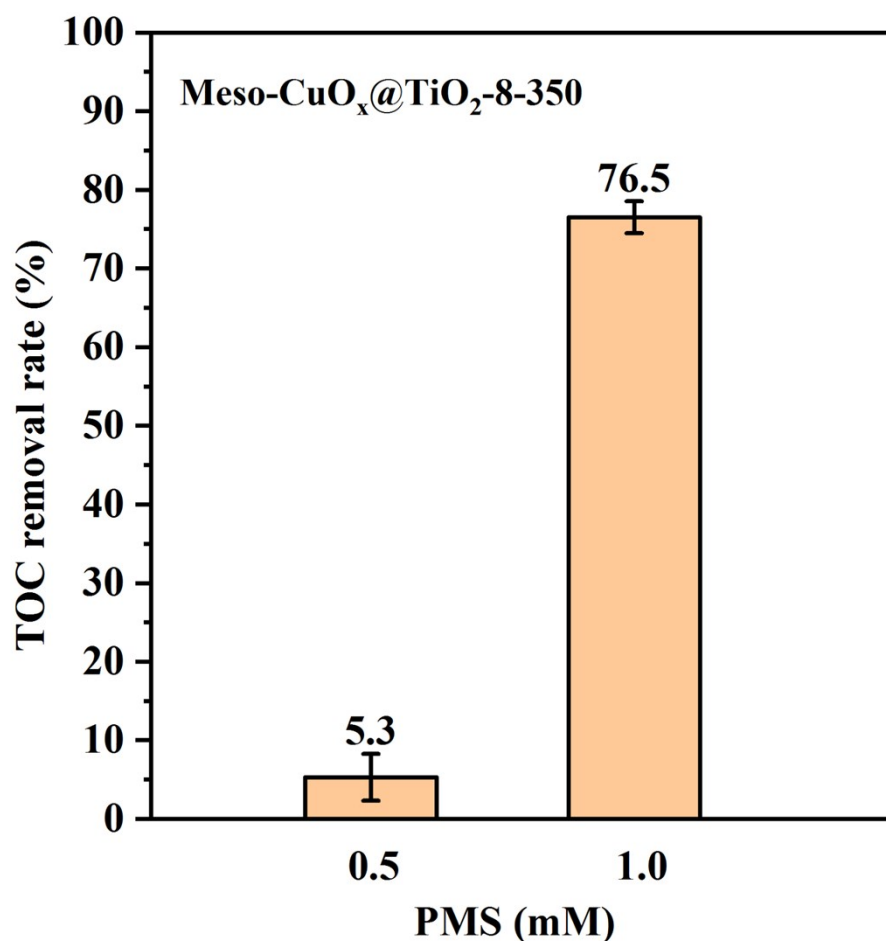


Fig. S7. The TOC removal percentages at 60 min during the MB degradation process using the Meso-CuO_x@TiO₂-8-350/PMS/light system with different PMS concentrations.

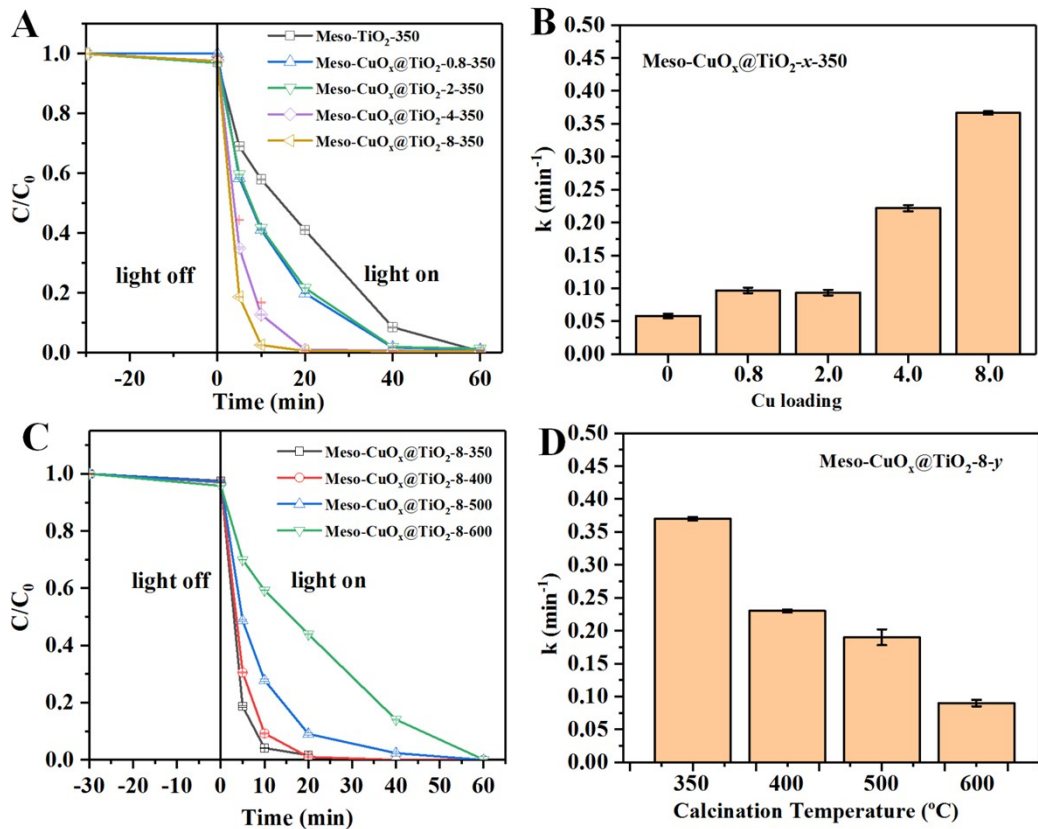


Fig. S8. MB degradation profiles (A, C) and the corresponding pseudo first order reaction kinetic constants (B, D) by using the catalyst/PMS/light systems over the samples with different Cu loadings and calcined at various temperatures.

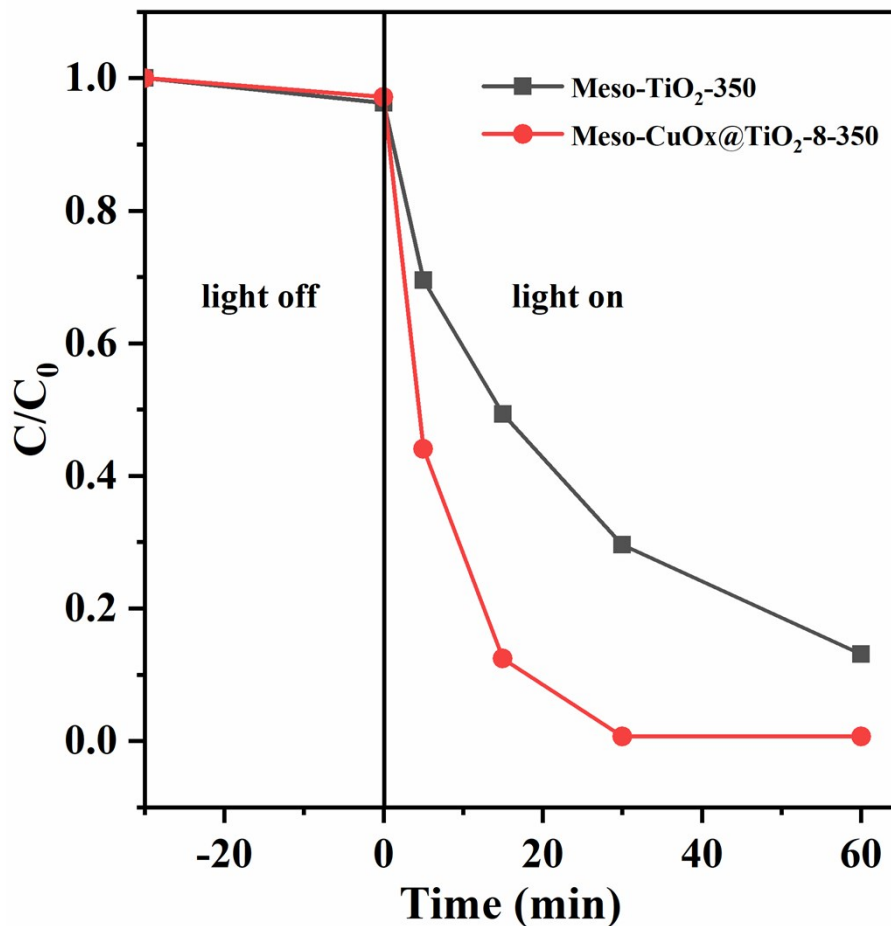


Fig. S9. Phenol degradation profiles by using the catalyst/PMS/light systems over the samples of Meso-CuO_x@TiO₂-8-350 and Meso-TiO₂-350.

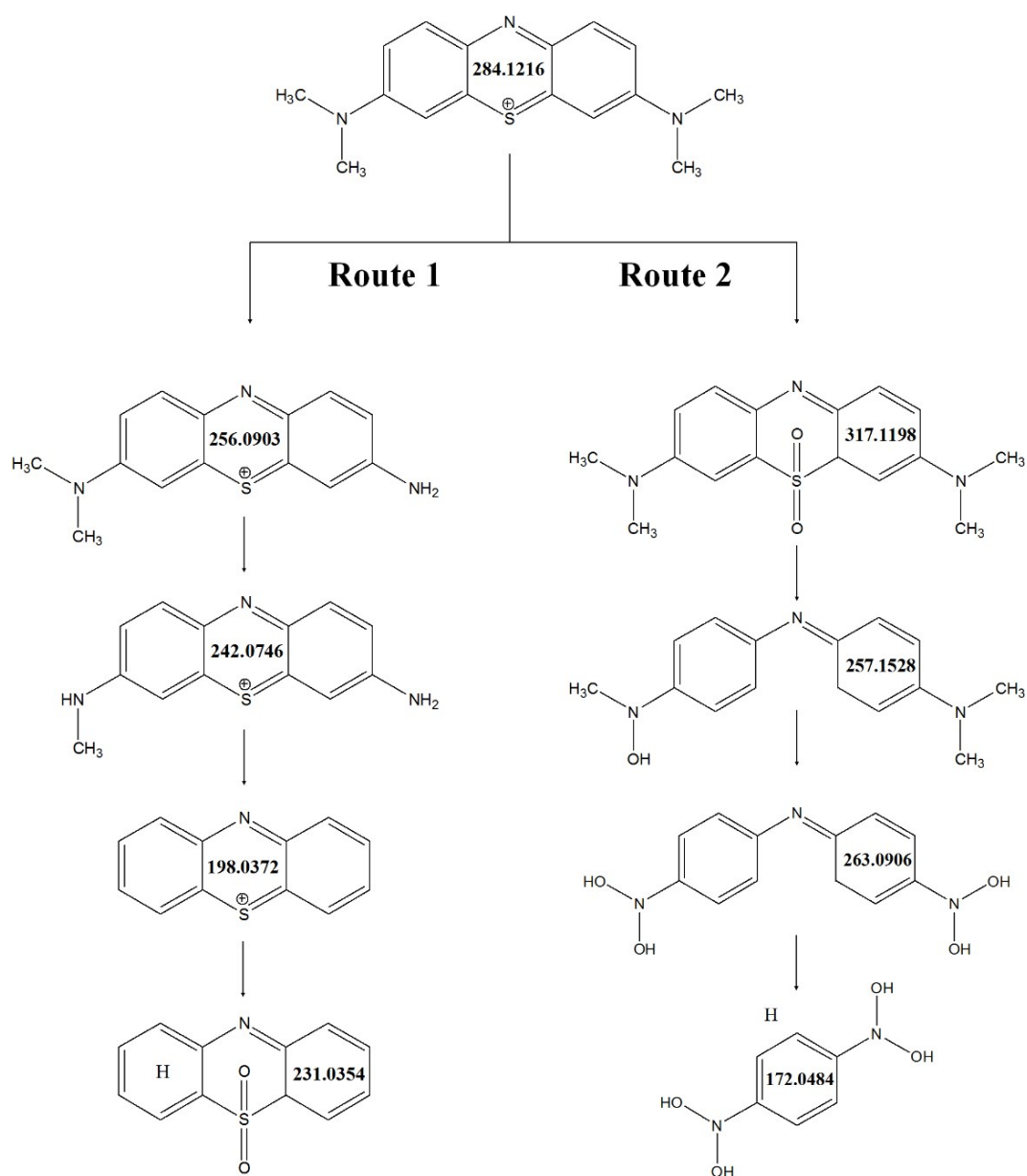


Fig. S10. The possible degradation pathway of MB in the Meso-CuO_x@TiO₂-8-350/PMS/light system. All the intermediates in this scheme have been captured in the LC-QTOF-MS experiments.

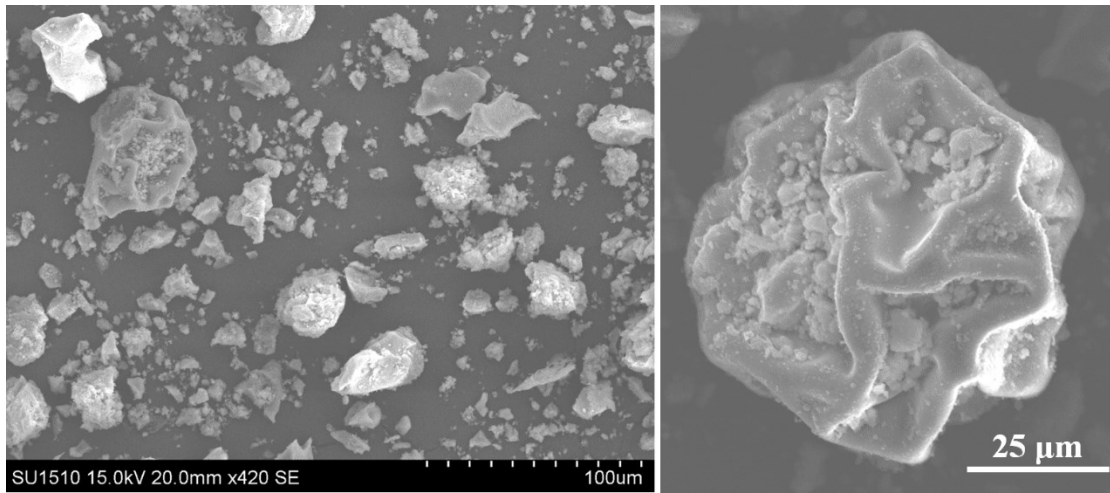


Fig. S11. SEM image of Meso-CuO_x@TiO₂-8-350 after cyclic use.

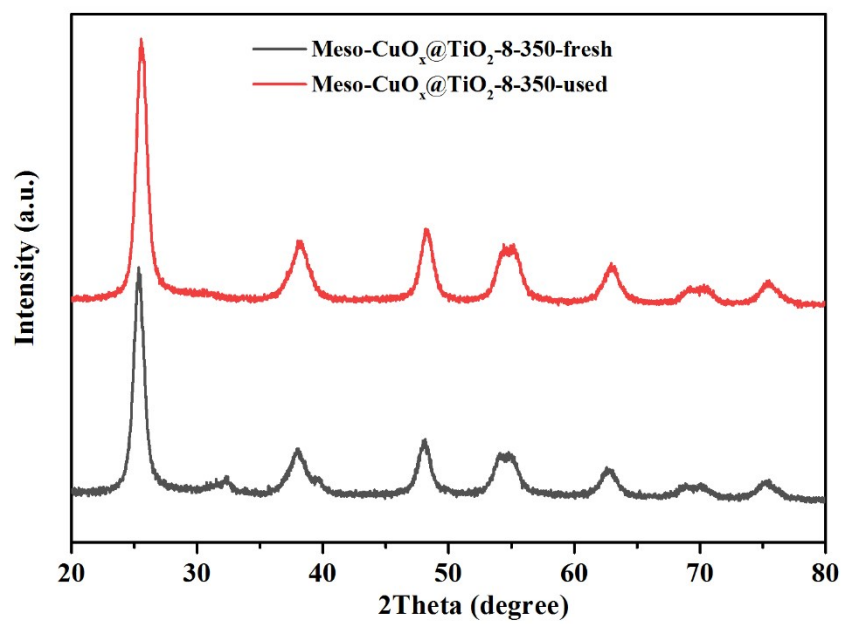


Fig. S12. The XRD patterns of Meso-CuO_x@TiO₂-8-350 before and after cyclic use.

Table S1. Summary of the textural properties of various samples with various Cu loadings obtained by calcination in air under different temperatures.

Sample	S_{BET} ($\text{m}^2 \text{g}^{-1}$)	Pore size (nm)	Pore volume ($\text{cm}^3 \text{g}^{-1}$)
Meso-TiO ₂ -350	147	7.7	0.28
Meso-CuO _x @TiO ₂ -0.8-350	117	8	0.25
Meso-CuO _x @TiO ₂ -2-350	154	7	0.29
Meso-CuO _x @TiO ₂ -4-350	137	9.5	0.39
Meso-CuO _x @TiO ₂ -8-350	131	8.1	0.37
Meso-CuO _x @TiO ₂ -8-400	79	21	0.35
Meso-CuO _x @TiO ₂ -8-500	34	38	0.26
Meso-CuO _x @TiO ₂ -8-600	13	59.5	0.13

Table S2. Test parameters and performance comparison for MB degradation through heterogeneous PMS activation

PMS dosage (mM)	Catalyst	MB concentration (mg L⁻¹)	Catalyst dosage (g L⁻¹)	Complete degradation time (min)	Ref.
0.74	MIL-101(Fe)	10	0.4	25	1
0.8	CuFe ₂ O ₄ @GO	20	0.2	30	2
2	CuCo-MOF-74	64	0.05	30	3
0.65	C-N-S	8	0.2	30	4
3.188	graphene	10 ¹	0.2	60	5
20	Fe ₃ O ₄ @MnO ₂	30	0.3	30	6
0.5	Meso-CuO _x @TiO ₂ -8-350	20	0.5	10	This study

References

1. Z. Xiao, Y. Li, L. Fan, Y. Wang and L. Li, *J. Colloid Interf. Sci.* 2021, **589**, 298-307.
2. X. Lei, M. You, F. Pan, M. Liu, P. Yang, D. Xia, Q. Li, Y. Wang and J. Fu, *Chin. Chem. Lett.* 2019, **30** (12), 2216-2220.
3. H. Li, Z. Yang, S. Lu, L. Su, C. Wang, J. Huang, J. Zhou, J. Tang and M. Huang, *Chemosphere* 2021, **273**, 129643.
4. W.-D. Oh, J. R. J. Zaeni, G. Lisak, K.-Y. A. Lin, K.-H. Leong and Z.-Y. Choong, *Chemosphere* 2021, **277**, 130313.
5. H. Sun, S. Liu, G. Zhou, H. M. Ang, M. O.Tade and S. Wang, *ACS Appl. Mater. & Interf.* 2012, **4** (10), 5466-5471.
6. S. Zhang, Q. Fan, H. Gao, Y. Huang, X. Liu, J. Li, X. Xu and X. Wang, *J. Mater. Chem. A* 2016, **4** (4), 1414-1422.